International Journal of Scientific Engineering and Science
Volume 4, Issue 1, pp. 32-36, 2020. ISSN (Online): 2456-7361

Comparison between the Numerical Modelization Result and Experimental Pressure of Journal Bearing

Thi Thanh Hai Tran[1], Anh Dung Le[1]
[1]School of Mechanical Engineering, Hanoi University of Science and Technology, Hanoi, Vietnam

Abstract*—This paper presents the comparison between the numerical modelization result pressure and the experimental pressure of the lubricated oil film for the hydrodynamic bearing. The pressure is calculated based on solving the Reynolds equation, the oil film thickness equation, and the equilibrium of the charge equation. These equations are discretized by a finite element mesh and are solved by using Newton-Raphson processes. The measured pressure of the oil film is determined at five different positions on the cross-section in the middle of the bearing according to the perimeter by pressure sensors. The results show the good agreement on the film pressures. However, the more load applied, the greater difference in value between the maximum of calculated pressure and measured pressure. When the rotation speed increases, the decrease in experimental pressure is more than the decrease in calculated pressure. The minimum pressure is slightly varied.*

***Keywords*—** *Lubrication, journal bearing, oil film pressure.*

I. INTRODUCTION

Hydrodynamic lubrication is of great interest to scientific researchers all over the world. In the 1930s, the researches of Swift [1] postulated boundary conditions for stability of journal bearings which are known as Swift- Stieber boundary conditions. They have been widely used in lubrication calculation. Chaitanya K Desai and Dilip C Patel [2] modeled and conducted experiments to create the pressure distribution of a hydrodynamic bearing under different loads and at different velocities. The calculation and experiments showed the maximum pressure where the thickness of the oil film is found to be the minimum and the zero pressure in the interrupted zone of the oil film. In the work by S. Kasolang Kasalung and M. Ali Ahmad [3] they performed experiments to investigate temperature effect of hydrodynamic bearing subjected to the different loads at the same velocity, the results indicate that increase of load at the same velocity can cause the higher temperature of the bearing. The highest temperature is at the zone with the minimum thickness of the oil film and descends in both sides (even in the interrupted zone of oil film and temperature also decreases as a nonlinear function). In 2001, N.X Toan et al. [4] created an automatic calculation program of hydrodynamic lubrication for journal bearings taking into account the shape and geometrical errors of the bearings. The problem was solved on the basis of the equation of oil film thickness called Reynolds equation under the Somerfield boundary conditions. The results exhibit the errors of shape and geometry of the bearings significantly decrease the pressure distribution leading to lower load capacity. In 2006, Tran Thi Thanh Hai [5] carried out a study on hydrodynamic lubrication for the connecting-rod bearing with regarding to elastic deformation effect of the matting surface. In 2014, Luu Trong Thuan et al. [6] built up an automatic computer program to calculate lubrication characteristics for bearings with regarding to the interrupted oil film thickness. The study used Reynolds's boundary conditions to solve Reynolds equation using Elrod algorithm. The result showed that pressure corresponding to the minimum thickness of the oil film non-zero, the zone of the interrupted oil film is indirectly found. For the different cross- sections of the bearings, the zone of interrupted oil film is found, to be maximum in the middle cross-section of the bearing and decreases for both sides. In 2019, Tran T. T. Hai and et al. [7] studied the influence of the radial clearance on the pressure distribution of the 5S-FE engine's connecting-rod big end bearing. The radials of the connecting-rod are measured at different screw tightening.

In this paper, we analyze the lubricated oil film pressure of the journal bearing at the different loads and at different rotation speed. The calculated pressure will be compared with the measurement pressure.

II. NUMERICAL MODELIZATION

The lubrication problem of the hydrodynamic bearing is solved base on solving the Reynolds equation, the oil film thickness equation at the dynamic regime. Fig. 1 is the middle section according to the length of the bearing. The load W is applied on the housing bearing. Oil supply hole is located on the housing and at the angle 45^o respected to the load direction. At the symmetric position is the oil return hole. The diameter of these holes is 5mm.

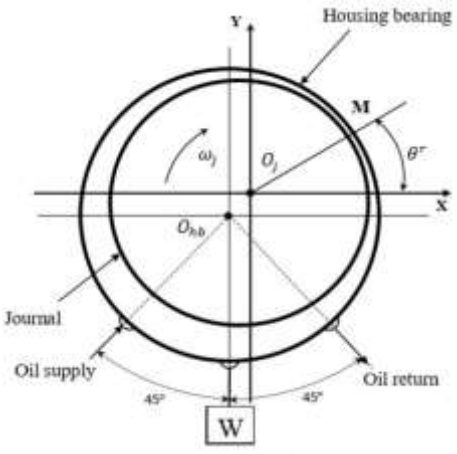

Fig. 1. Plane section of bearing.

The Reynolds equation is [8]:

International Journal of Scientific Engineering and Science
Volume 4, Issue 1, pp. 32-36, 2020. ISSN (Online): 2456-7361

$$\frac{\partial}{\partial x}\left(h^3\frac{\partial p}{\partial x}\right)+\frac{\partial}{\partial z}\left(h^3\frac{\partial p}{\partial z}\right)=6\mu v\frac{\partial h}{\partial x} \quad (1)$$

where: p is the oil film pressure, h is the oil film thickness, x and z are circumference and bearing length direction.

The boundary conditions used to solve the Reynolds equation are based on the separation of the active zone Ω and inactive zone (cavitation zone) Ω_o. In the active zone, the pressure is established and equilibrated with the applied load. In the inactive zone, the pressure (p_{cav}) is lower than the atmospheric pressure. The Fig. 2 presents the active zone and inactive zone in the film domain.

Active zone: $p > p_{cav}$

Inactive zone: $p = p_{cav}$; $p_{cav} < 0$

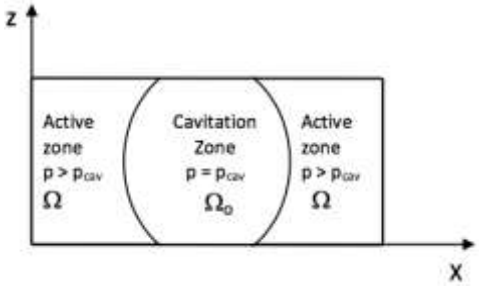

Fig. 2. The active zone and the inactive zone in the film domain

With the dimensionless parameters:

$$\theta=\frac{x}{R};\ \zeta=\frac{z}{R};\ H=\frac{h}{C};P=\frac{p}{6\mu\omega\left(\frac{R}{C}\right)^2}.$$

We obtained the dimensionless Reynolds equation:

$$\frac{\partial}{\partial\theta}\left(H^3\frac{\partial P}{\partial\theta}\right)+\frac{\partial}{\partial\zeta}\left(H^3\frac{\partial P}{\partial\zeta}\right)=\frac{\partial H}{\partial\theta} \quad (2)$$

The film thickness equation:

$$H(\theta')=1-\varepsilon_x\cos\theta-\varepsilon_y\sin\theta \quad (3)$$

The forces acting on the oil film is represented by the following formula:

$$f=\begin{Bmatrix}F_x(\bar{x},\bar{y})\\F_y(\bar{x},\bar{y})\end{Bmatrix}=\sum_{\Omega}\begin{Bmatrix}\iint_{\Omega}-P.\cos\theta d\theta d\zeta\\\iint_{\Omega}-P.\sin\theta d\theta d\zeta\end{Bmatrix}=\begin{Bmatrix}w_x\\w_y\end{Bmatrix}=w \quad (4)$$

with $\bar{u}=(\bar{x},\bar{y})$ is the vector (ε_x, ε_y)

f is the vector of the hydrodynamic force.

w is the vector of the external force

A. Discretization of the Reynolds Equation

The film is discretized by quadrangular elements with four nodes (Fig.3).

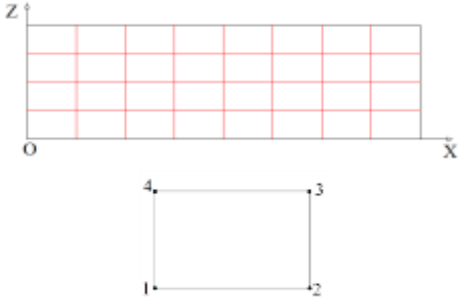

Fig. 3. Solid surface mesh

The pressure at the point in the element is calculated:

$$P=\sum_{i=1}^{n}P_iN_i=P^T\{N_i\} \quad (5)$$

Thus $\partial P_e=\partial N_i\{P_i\}$ and the left side of the (2) is written as:

$$VT=\{M_e\}=\iint_{S_e}\frac{\partial\{N_i\}}{\partial\theta}H_e^3\frac{\partial N_i}{\partial\theta}\{P_i\}d\theta d\zeta+$$

$$+\iint_{S_e}H_e^3\frac{\partial\{N_i\}}{\partial\zeta}\frac{\partial N_i}{\partial\zeta}\{P_i\}d\theta d\zeta$$

The right side of the (2) is:

$$VP=\{B_e\}=-\iint_{S_e}\{N_i\}.\frac{\partial H_e}{\partial\theta}dS_e$$

Assemble the elements we obtain the equation for the whole mesh:

$$M.P=-B \quad (6)$$

By solving (3), we obtain the pressure for the oil film.

B. Discretization of the Equilibrium of the Charge

Substitution (5) into the left-side of (4), we have:

$$f=\begin{Bmatrix}F_x(\bar{x},\bar{y})\\F_y(\bar{x},\bar{y})\end{Bmatrix}=\sum_{\Omega}-\begin{Bmatrix}P^T\iint_{\Omega}N.\cos\theta d\theta d\zeta\\P^T\iint_{\Omega}N.\sin\theta d\theta d\zeta\end{Bmatrix} \quad (7)$$

In the formula (7), we take:

$$S=\iint_{\Omega}N.\cos\theta d\theta d\zeta;R=\iint_{\Omega}N.\sin\theta d\theta d\zeta \quad (8)$$

Jacobian matrix of the force vector:

$$J_{\bar{u}}f(\bar{u})=\begin{bmatrix}\frac{\partial F_x(\bar{x},\bar{y})}{\partial\bar{x}}&\frac{\partial F_x(\bar{x},\bar{y})}{\partial\bar{y}}\\\frac{\partial F_y(\bar{x},\bar{y})}{\partial\bar{x}}&\frac{\partial F_y(\bar{x},\bar{y})}{\partial\bar{y}}\end{bmatrix} \quad (9)$$

Replace (8) into (9), we get:

$$J_{\bar{u}}f(\bar{u})=-\begin{Bmatrix}S^T\\R^T\end{Bmatrix}\begin{bmatrix}P_{\bar{x}}&P_{\bar{y}}\end{bmatrix}=-\begin{bmatrix}S^TP_{\bar{x}}&S^TP_{\bar{y}}\\R^TP_{\bar{x}}&R^TP_{\bar{y}}\end{bmatrix}$$

where $P_{\bar{x}}=\frac{\partial P}{\partial\bar{x}};P_{\bar{y}}=\frac{\partial P}{\partial\bar{y}}$

Rewrite (3) as:

$$M(\bar{x},\bar{y})P=-B(\bar{x},\bar{y}) \quad (10)$$

Derivative (9) respect to the components $\bar{x},\bar{y}$ we obtain:

$$M\left[P_{\bar{x}},P_{\bar{y}}\right]=\left[-M_{\bar{x}}P+B_{\bar{x}},M_{\bar{y}}P+B_{\bar{y}}\right] \quad (11)$$

where $M_{\bar{x}}=\frac{\partial M}{\partial\bar{x}},M_{\bar{y}}=\frac{\partial M}{\partial\bar{y}};B_{\bar{x}}=\frac{\partial B}{\partial\bar{x}};B_{\bar{y}}=\frac{\partial B}{\partial\bar{y}}$

International Journal of Scientific Engineering and Science
Volume 4, Issue 1, pp. 32-36, 2020. ISSN (Online): 2456-7361

$$\begin{cases} \dfrac{\partial B_i}{\partial \bar{x}} = \iint\limits_{\Omega} N_i \sin\theta d\theta d\zeta, \dfrac{\partial B_i}{\partial \bar{y}} = -\iint\limits_{\Omega} N_i \cos\theta d\theta d\zeta \\ \dfrac{\partial M_{ij}}{\partial \bar{x}} = \iint\limits_{\Omega} H^2 \cos\theta \left(\dfrac{\partial N_i}{\partial \theta}\dfrac{\partial N_j}{\partial \theta} + \dfrac{\partial N_i}{\partial \zeta}\dfrac{\partial N_j}{\partial \zeta} \right) \mathrm{d}\theta\,\mathrm{d}\zeta \\ \dfrac{\partial M_{ij}}{\partial \bar{y}} = \iint\limits_{\Omega} H^2 \sin\theta \left(\dfrac{\partial N_i}{\partial \theta}\dfrac{\partial N_j}{\partial \theta} + \dfrac{\partial N_i}{\partial \zeta}\dfrac{\partial N_j}{\partial \zeta} \right) \mathrm{d}\theta\,\mathrm{d}\zeta \end{cases} \quad (12)$$

Solving the system of (11), we get the vector ($P_{\bar{x}}, P_{\bar{y}}$). Substitute it into (9) to obtain the Jacobi matrix $J_{\bar{u}} f(\bar{u})$. Then the vector $\bar{u} = (\bar{x}, \bar{y})$ is calculated from the interpolation steps according to the following formula:

$$\bar{u}^{(k+1)} = \bar{u}^{(k)} - J_{\bar{u}}^{-1} f(\bar{u}) \left[f(\bar{u}^{(k)}) - w \right] \quad (13)$$

III. Measurement of Oil Film Pressure

A. Experimetal Device

The experimental device used in this study respects the kinematics of bearing, including a shaft and a housing. The photography and functional scheme of the experimental device are presented on Fig. 4. An electric motor (2) transmits motion to the shaft (3) through the belt (4). The shaft is supported by two pillow blocks (5). The shaft, the housing bearing (6) and the oil film created when the shaft rotates together form the journal bearing in this study. The pressure sensors (12) are attached on the bearing to capture the real pressure in time at the different positions along the perimeter of the middle section of the bearing. The oil feed hydraulic system which consists of the oil tank (7), the oil pump (8), the directional controlling valve (9), the flow control valve (10), the pressure gauge (11), oil feed pipe and oil return pipe.

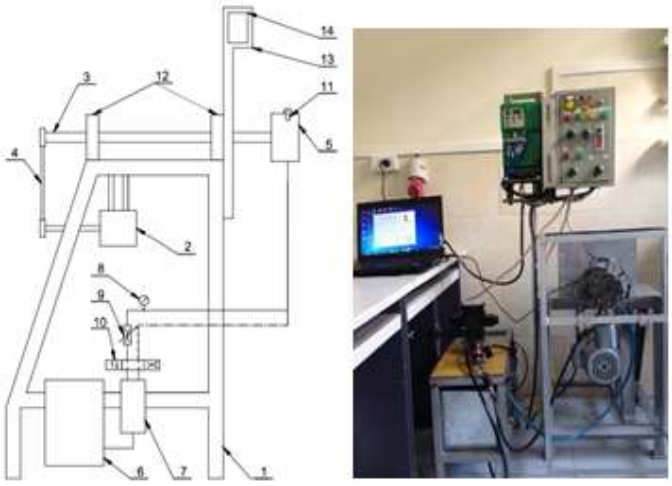

Fig. 4. Functional scheme and photography of experimental device

The Fig.5 shows the studied journal bearing. The part of the shaft, which its diameter D and length L, play the role as the journal of the journal bearing. During operation, the journal center is supposed to be unmoved and the housing center position is changed which makes the distance between these two centers varies depend on the value of applied load. However, the housing bearing can slightly rotate within rotating direction of the journal.

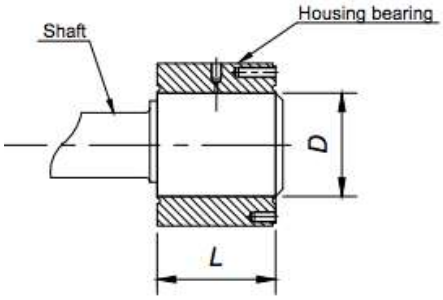

Fig. 5. Functional scheme and photography of experimental device.

The dimensions of the bearing as follows: length of the bearing L= 50 mm, diameter of the bearing D = 70 mm, precision of the shaft surface is up to 8 level, precision of the housing up to 6 level, the radial clearance C = 0,05 mm; lubricated oil with viscosity μ = 0,015 Pa.s; the density ρ=850 kg/m^3.

C. Experimental Method

The lubricated oil film pressure is measured at five different positions A1, A2 A3, A4, A5 on the middle cross-section in the middle of the bearing according to the perimeter by five pressure sensors MPXHZ6400A (Fig.6) [9]. The pressure of the oil film under different loads 140 N, 170 N and 200 N and different velocities 200 rpm, 400 rpm, 600 rpm. After starting the experimental device for 10 minutes, the first measurement is read, and after that the break time between measurements is 15 minutes. For each load level or velocity, the measurements were recorded eight times. The measurement results were analyzed by using technique for analysis of experimental data [13] (experimental sample variance calculation $S^2 = \sum_{k=0}^{8} (x^k - x)^2$ and average deviations) standard deviations of data sequence $S = \sqrt{S^2}$ from 0.07 to 0.15 shows that reliability of the chosen data [10].

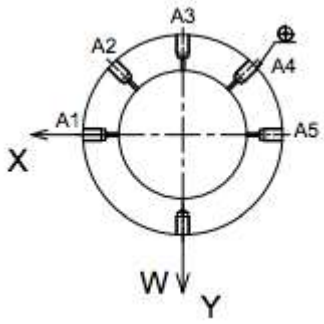

Fig. 6. Pressure sensor location

IV. The Results

With the algorithm presented in part 2, we program on Fortran software. Fig. 7 presents the numerical modelization pressures at the middle cross-section in the middle of the bearing according to the perimeter, the load of 200 N and the

International Journal of Scientific Engineering and Science
Volume 4, Issue 1, pp. 32-36, 2020. ISSN (Online): 2456-7361

velocities of 300 rpm, 400 rpm and 600 rpm. It shows that, the pressure is positive in the charge zone, from 0^o to 210^o of the housing bearing. When the rotation speed increases, the maximum value pressure is decreases and the zone pressure is larger. It can be explained that the minimum film thickness increases when the velocities increase.

Fig. 8 represents a comparison between numerical modelization pressure and measured in experiments at the load of 140 N and velocity of 300 rpm. When the bearing works, the bearing housing rotates an angle from the original. It means, the sensor positions also rotate an angle with the housing bearing. We note, the good agreement on the film pressure. However, the maximum pressure in the calculated is 66.5 KPa at 117^o of boring, the maximum in experiment is 64.7 KPa at the 105^o. That can be explained, the maximum pressure position of oil film is not the same as the position of pressure sensor. It means, the pressure reaches the maximum value at a position in the range from A3 to A4. The real maximum value of pressure is not measured.

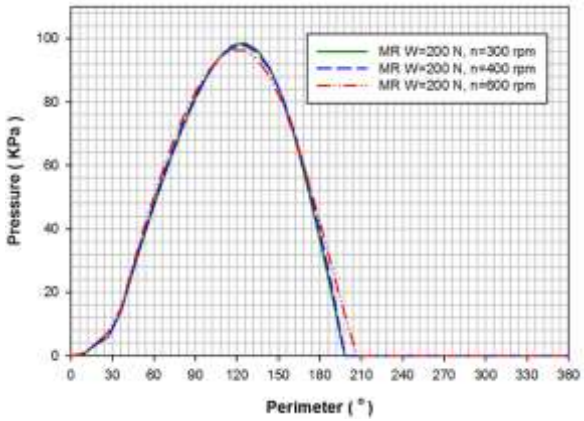

Fig. 6. Calculated pressure at the different rotation speeds, applied load of 200 N.

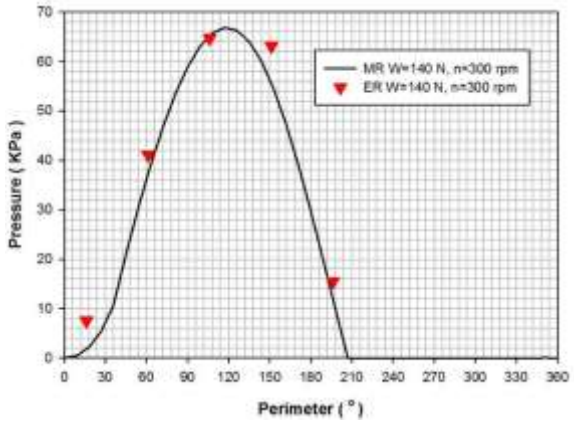

Fig. 8. Comparison the oil film pressure between the calculated results (MR) and measured results (ER) at the load W = 140 N, n=300 rpm.

Fig. 9 shows a comparison of oi film pressure in calculation and in experiment at different applied load and journal speed of 300 rpm. It shows that, the more load applied, the greater difference in maximum value between the of calculated pressure and measured pressure. At the loads of 140N, 170 N and 200 N, the maximum pressure of experiment is corresponding to 64.7 KPa, 76.1 KPa, 90 KPa and the numerical result is 65.5 KPa, 83.25 KPa, 96.03 KPa. Thus, it remains to suppose that the experimental device has an imperfection of operation which is not considered in the numerical simulation. The minimum pressure is slightly varied.

Fig. 10 represents a comparison the oil film pressure in numerical simulation and measured at the different rotational frequencies for the load applied of 200 N. The maximum pressures decrease when the velocity increase. However, the decrease in maximum calculated pressure is less than the decrease in experimental pressure. At the rotational frequencies of 300 rpm, 400 rpm, 600 rpm, the maximum calculated pressures are corresponding to 98.63 KPa, 97.2 KPa, 96.01 KPa and the experimental results are 65,5 KPa, 83.25 KPa, 96.03 KPa respectively. The minimum pressure is slightly varied.

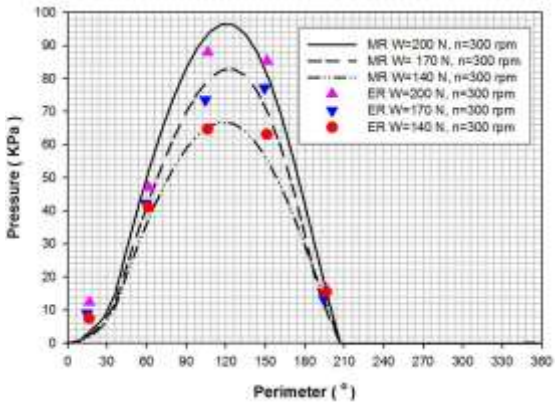

Fig. 9. Comparison the oil film pressure between the calculated results (MR) and measured results (ER) at the different load applied, 300 rpm.

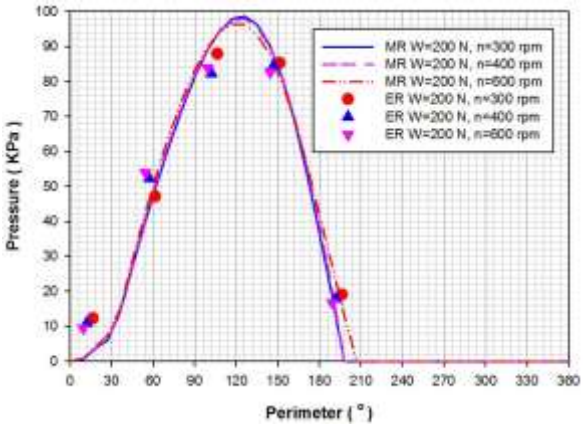

Fig. 10. Comparison the oil film pressure between the calculated results (MR) and measured results (ER) at the different speed journals, 200 N.

V. CONCLUSIONS

This research presents the comparison between the numerical modelization pressure and the experimental pressure of the lubricated oil film for the hydrodynamic bearings with circulating oils. The pressure is calculated based on solving the Reynolds equation and the oil film thickness equation, and the equilibrium of the charge equation which are discretized by a finite element mesh and are solved by using Newton-Raphson iterations. The measured pressure of the oil

film is determined at five different positions on the cross-section in the middle of the bearing according to the perimeter by pressure sensors.

The results show the good agreement on the film pressures. The pressure is positive in the charge zone, from 0^o to around 210^o of the housing bearing. However, the more load applied, the greater difference in value between the maximum of calculated pressure and measured pressure. Thus, it remains to suppose that the experimental device has an imperfection of operation which is not considered in the numerical simulation. The minimum pressure is slightly varied.

The maximum pressures decrease when the velocity increase and the pressure zone is larger. However, the decrease in experimental pressure is more than the decrease in calculated pressure. The minimum pressure is slightly varied.

REFERENCES

[1] Swift, H. W., The Stability of Lubricating Films in Journal Bearings, Proc.-Inst. Civ. Eng., 233, pp. 267–288, 1932.

[2] Chaitanya K Desai& Dilip C Patel, "Experimental analysis of pressure distribution hydrodynamic journal bearing: A parametric study", *International Conference on Mechanical Engineering 2005*, 2005.

[3] S. Kasolang Kasalung, M. Ali Ahmad, "Experimental study of temperature profile in a journal bearing", *1st Joint International Symposium on System-Integrated Intelligence*, 2012

[4] Nguyen Xuân Toan, Tran Thi Thanh Hai, Dương Minh Tuan, "Building the automatic computing program for hydrodynamic lubrication bearings with researching the shape geometrical errors of bearings", the *19th Scientific Conference of HUST*, pp 83-87, Hanoi, 2001.

[5] Thi Thanh Hai Tran, T. Zeghloul, D. Bonneau, "Experimental of the interaction between the different bodies of a connecting-rod big end bearing", World Congress, Besancon, june 18-21, 2007.

[6] Dinh Tan Nguyen, Trong Thuan Luu, Thi Thanh Hai Tran, "Built up an automatic computer program to calculate lubrication characteristics for bearings with regarding to the oil film disruption", *Vietnam Mechanical Engineering Magazine*, No 3, 2014.

[7] Tran Thi Thanh Hai, Nguyen Dinh Tan, Luu Trong Thuan, "Influence of the radial clearence on the pressure distribution of the 5S-FE engine's connecting-rod big end bearing", *Journal of Science and Technology Technical University*, No.132 (2019), pp 40-45, 2019

[8] Bonneau D., Fatu A., Shouchet D., "Hydrodynamic Bearings", ISTE, London and John Wiley & Sons, New York, 2014.

[9] Trung Thien PHAM, Thị Thanh Hai TRAN, 2015 "Development a supervise system of pressure and temperature hydrodynamic bearing", *Proceedings of the 4th National Conference on Mechanical Sciences & Technology*, November 06, 2015.

[10] Nguyen Doan Y, "Experimental data processing in engineering", *Publishing of Science and Engineering*, Vietnam, 2019.